Mechanical properties of low-alloy-steels with bainitic microstructures and varying carbon content

A Weber[1,5], J Klarner[2], T Vogl[2], R Schöngrundner[2], G Sam[3] and B Buchmayr[4]
[1] Materials Center Leoben Forschungs GmbH, Roseggerstraße 12, A-8700 Leoben
Email: andreas.weber@unileoben.ac.at, Österreich
[2] voestalpine Tubulars GmbH &Co KG, Kindberg, Österreich
[3] RAG Rohöl-Aufsuchungs Aktiengesellschaft, Wien, Österreich
[4] Chair of Metal Forming, Department of Product Engineering, Montanuniversitaet Leoben, Österreich

Abstract. Materials used in the oilfield industry are subjected to special conditions. These requirements for seamless steel tubes are between the priorities of strength, toughness and sour gas resistance. Steels with bainitic microstructure provide a great opportunity for those harsh environmental conditions. With different morphologies of bainite, like carbide free, upper or lower bainite, the interaction of high tensile strength and elongation is assumed to be better than with tempered martensite. To form carbide free bainite two ways of processing are proposed, isothermal holding with accurate time control or controlled continuous cooling. Both require knowledge of time-temperature transformation behaviour, which can be reached through a detailed alloying concept, focused on the influence of silicon to supress the carbide nucleation and chromium to stabilize the austenite fraction. The present work is based on three alloys with varying silicon and chromium contents. The carbide free microstructure is obtained by a continuous cooling path. Additionally different heat treatments were done to compare the inherent performance of the bainitic morphologies. The bainitic structures were characterized metallographically for their microstructure and the primary phase by means of transmission electron microscopy. The mechanical properties of carbide-free structures were analysed with quasi-static tensile tests and Charpy impact tests. Moreover, investigations about hydrogen embrittlement were done with focus on the effect of retained austenite. The results were ranked and compared qualitatively.

1. Introduction

Contemporary developments in the steel industry promise extraordinary balance of strength and toughness. It emphasizes the material as an essential part of modern applications [1]. Seamless steel tubes as an important part are used in structural, mechanical and engineering fields. The largest market share for seamless steel tubes contains oil country tubular good (OCTG) and line pipes [2]. The tense political situation in the Middle East and the changed economic market in summer 2015, led to downgraded forecasts for the demand of steel tubes [2], but investigation and exploitation of unconventional sources of oil will lead to a long-term increased demand [3]. Tools for the oil industry have to fulfil a variety of mechanical and chemical requirements [4], which are influenced by the natural conditions and the drilling techniques. Following requirements are postulated in the literature [5]:

- highest tensile strength,
- low yield-to-tensile ratio,
- high impact toughness at low temperatures (-20 / -40 °C),
- resistance against hydrogen induced cracking (HIC).

The aim of this contribution is to rank low-alloy carbon steels with high strength microstructures to check their practical usability for OCTG production.

1.1. Production route

The typical production for seamless steel tubes includes a subseries of billet heating, cross rolling and piercing, push bench processing, reheating, stretch reduction, elongation and (accelerated) water cooling [6, 7]. Seamless pipes for applications in the oil and gas industry are typically made in the quenched and tempered martensitic condition as it is defined in the widely used API (American Petroleum Institute) standard [8]. For premium qualities, improvements are performed by thermomechanical processing [6].

1.2. Sour gas resistance

Sour gas is a natural or any other gas containing significant amounts of hydrogen sulphide (H_2S). Steel is damaged by sour gas by the loss of ductility and formation of cracks. The free hydrogen H^+ is hindered to recombine at the material surface by the HS^- from the dissociated H_2S. So, it can diffuse into the material and remains at dislocations, phase boundaries and cracks, where it recombines with other H^+ to H_2. This leads to local pressure and propagates cracks and embrittlement [9, 10].

2. Alloy design

The alloys of the present study are focused on martensitic and bainitic morphologies with varying silicon- and chromium contents. The chemical compositions of the investigated materials are shown in table 1. The carbon content in alloy 3 is slightly lowered in comparison with alloy 1 and 2. The silicon content from alloy 2 is by half the content of alloy 1 and 3, the chromium content of alloy 3 is a little bit higher than those of alloy 1 and 2.

Table 1. Chemical composition of the investigated steels with martensite-start-temperature (M_s).

	C [wt%]	Si [wt%]	Mn [wt%]	Cr [wt%]	Mo [wt%]	B [ppm]	M_s [°C]
Alloy 1	0.25-0.3	0.5-1.0	1.0-1.5	0.5-1.0	0.3-0.7	5-10	360
Alloy 2	0.25-0.3	0.1-0.5	1.0-1.5	0.5-1.0	0.3-0.7	5-10	364
Alloy 3	0.2-0.25	0.5-1.0	1.0-1.5	1.0-1.5	0.3-0.7	5-10	380

The transformation points for martensite-start, bainite-start, lower-bainite-start and A_{c3} were estimated with thermodynamical calculations after Buchmayr, 2002 [11]. Based on these calculations the austenitization temperature was set 50 °C higher than A_{c3} (alloy 1 = 940 °C, alloy 2 = 910 °C, alloy 3 = 950 °C) and the holding time at this temperature was fixed with 5 minutes. The alloying concept was validated with the thermodynamic calculation software JMatPro. The melts in laboratory scale were produced (casted, rolled) at voestalpine Stahl GmbH in Linz. Jominy tests have proved a good hardenability of all three alloys. Continuous and isothermal time-temperature diagrams were carried out by a dilatometer Bähr DIL805A at the Chair of Physical Metallurgy and Metallic Materials of the Montanuniversitaet Leoben. The CCT and the TTT-Diagram of alloy 1 are shown in figure 1.

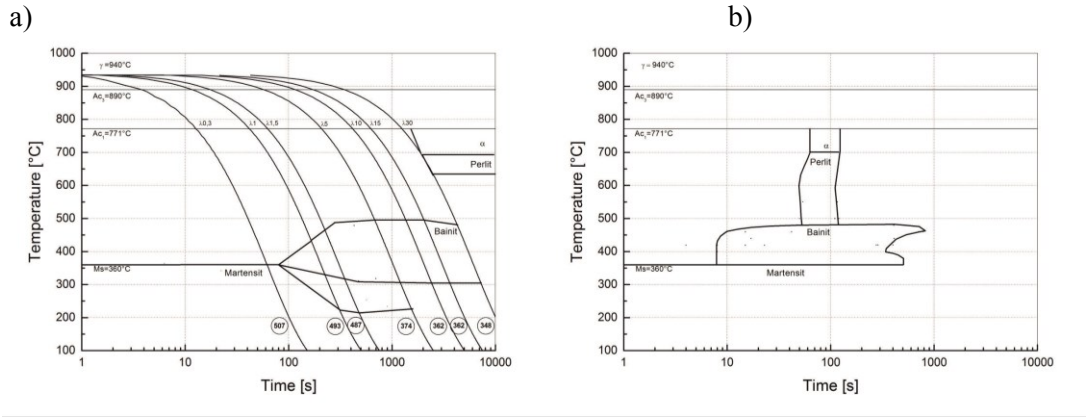

Figure 1. a) CCT diagram of alloy 1, b) TTT diagram of alloy 1.

3. Experimental

3.1. Mechanical properties

The mechanical properties were determined using tensile tests according to DIN EN 10002-1 and Charpy V-notch impact tests according to DIN EN 10 045-1. The dimensions for the round tensile specimens are shown in figure 2 a). The experiments were carried out on a universal testing machine Zwick/Roell 250 at the Chair of Metal Forming at the Montanuniversitaet. The deformation analysis was done with the optical measurement system GOM-Aramis. With this method it is possible to track the whole deformation path and to identify local strains. Figure 2 b) shows an example of a sample with an overlaid analysis mask (coloured regions). The notch-impact tests were done at the Chair of Metal Forming with a pendulum impact tester from Zwick/Roell RKP 450 with a 300 J hammer.

3.2. Heat treatment

The Charpy specimens were heat treated with a Gleeble 3800 at the Chair of Metal Forming. The heat treatments for the tensile specimens were realized with the inductive FTTU (Fast Thermal Treatment Unit) from the Thermo-Mechanical Treatment Simulator Servotest at the Chair of Metal Forming. All heat treatments are listed in table 2. Four heat treatments were performed, one in as quenched condition with air pressure cooling (approximately 60 seconds to room temperature), a continuously cooled condition following a cooling curve with a defined factor λ2 (described in equation (1)), and two tempered conditions. For the quenched and tempered (Q&T) conditions two different cooling rates are performed (as quenched and λ2). The tempering was done with reheating 15 Ks^{-1} at 700 °C and holding for 10 minutes.

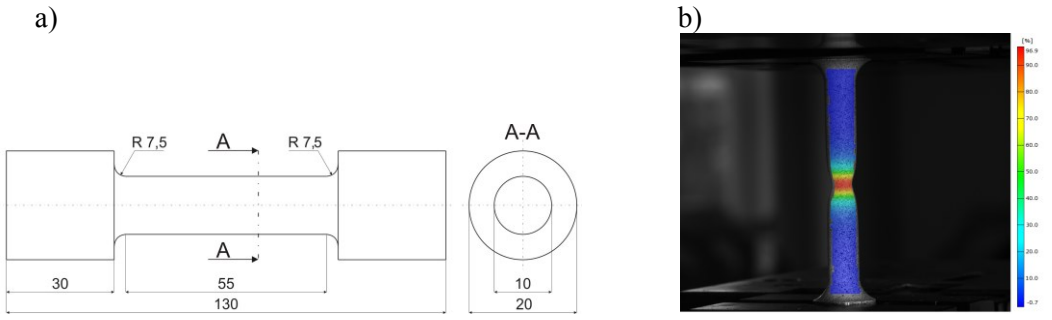

Figure 2. a) Round specimen for tensile test according to DIN EN 100002-1, b) image of the tensile test with optical measuring system GOM-Aramis.

Table 2. Matrix of heat treatments.

Alloy 1	Alloy 2	Alloy 3
as quenched	as quenched	as quenched
λ2	λ2	λ2
λ2 tempered 700°C 10’	λ2 tempered 700°C 10’	λ2 tempered 700°C 10’
Q&T 700°C 10’	Q&T 700°C 10’	Q&T 700°C 10’

The variable λ (equation (1)) describes the time for the degressive course of the cooling-rate:

$$\lambda = \frac{t_{800°C} - t_{500°C}}{100} \qquad (1).$$

Finite element thermal calculations indicated for tube thicknesses between 8 and 24 mm, an average cooling rate in air after the hot rolling mill with a finish rolling temperature between 950–1000 °C of about 0,1–0,5 Ks^{-1} [8]. This leads to a cooling time of approximately 30 minutes and a λ value of about 2, carried out by dilatometric experiments.

3.3. Hydrogen Induced Cracking

In addition to the mechanical properties a first estimation of sour service resistance against hydrogen induced cracking were done. Therefore the standard testing method from the NACE Standard TM0284-2011 [12] was modified for smaller samples. The selected samples were laid in a sour-gas environment with defined temperature, chemical composition of the medium and pH-value for 96 hours. After penetration the cross section of the sample is examined with a light microscope (100 x magnification). The identified cracks were measured as shown in figure 3 and related with the crack sensitive ratio (CSR), given in equation (2):

$$CSR = \frac{\sum(a * b)}{(W * T)} * 100\,\% \qquad (2).$$

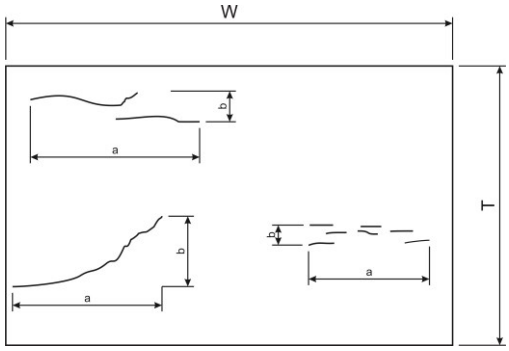

Figure 3. Schematic illustration of sour gas-cracks for HIC evaluation, a = crack length, b = crack thickness, W = section width, T = test specimen thickness.

3.4. Investigations with transmission electron microscope

To confirm the produced microstructures transmission electron microscope (TEM) investigations were made at the Alloy Development Group Seibersdorf (Dr. Krystina Spiradek-Hahn).

TEM samples were prepared by mechanical thinning and electrolytic polishing. Investigations were done with the transmission electron microscope Philips CM20 STEM and Tecnai F20 (high definition) with acceleration voltage of 200 kV.

4. Results and discussion

4.1. Microstructure

It could be shown that for all alloys the as quenched conditions lead to a mainly martensitic morphology with different amounts of retained austenite and some carbides between the laths. Alloy 3 exhibits more coarse carbide-precipitations and partially self-tempered martensite. Figure 4 shows the morphology of alloy 1 and 3 for the as quenched conditions. The dark areas in a) are the martensite-laths, the thick bright dappled needle is a bainite lath. Figure 4 b) shows crossed precipitations, which are typical for tempered martensite. This phenomenon can be explained with the high martensite-start temperature of alloy 3 (listed in table 2) and the reduced carbon content. The first laths are formed at high temperatures, when the carbon has enough time to diffuse and to form precipitations [13]. The light grey film along the grain boundary is identified as retained austenite.

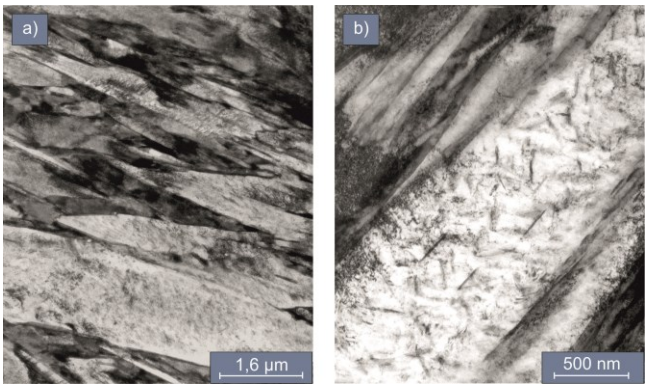

Figure 4. TEM micrographs, as quenched conditions, a) alloy 1, b) alloy 3.

For alloy 1 and 3 carbide free bainite could be identified at the continuously cooled conditions with λ2. Light microscope images show a similar structure for alloy 3, but the carbide free morphology is not investigated with TEM. Figure 5 shows the TEM micrograph from alloy 1 with the related diffraction image. Attributable to the lower austenitization temperature it could be seen, that the microstructure of alloy 1 is finer and more structured than alloy 3. It is worth to note, that the microstructures are primarily carbide free bainite, but related to the cooling conditions further bainitic morphologies can occur.

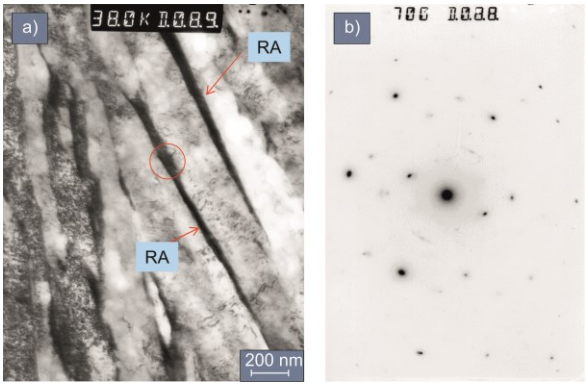

Figure 5. Alloy 1 continuously cooled at λ2 condition, a) TEM micrograph of alloy 1, RA=retained austenite, b) diffraction image to verify the carbide free morphology.

4.2. Mechanical properties and hydrogen resistance

Mechanical properties of the alloys with their different morphologies were determined with tensile and Charpy V-notch tests. The results of the tensile tests are shown in table 3. The as quenched conditions show the highest values compared to the other conditions with reduction of area-values close to 40 %. The total elongation of alloy 3 as quenched is 6 % and lies significantly below the elongation of alloy 2 as quenched and alloy 1 as quenched which is 9.5 % and 11% respectively. Regarding to sour gas resistance the CSR values from the as quenched conditions are generally lower in comparison to the other morphologies. It is surprising, that alloy 2 with the highest tensile strength has a lower CSR than alloy 1. This is caused by the lower silicon- and the reduced boron-content in the alloying concept. Alloy 3 shows the lowest crack sensitive ratio. This may be caused by the higher chromium content with respect to the lowered carbon content. It is considered that chromium improves the hydrogen embrittlement resistance by contributing to improve the hydrogen trapping capability and to inhibit the crack propagation. Comparison of impact toughness to tensile strength shows the correlation between these factors. By decreasing strength the impact energy increases significantly. The values of the carbide free (λ2) and carbide free tempered morphologies (λ2&T 700°C 10 minutes) were surprising. Alloy 1, with the highest carbon and silicon content, shows the highest strength with 1413 MPa and 1043 MPa with the lowest total elongation of 9.6 % and 10.5 % respectively in both conditions. The reduction of area, with 52 % and 47 % is lower than for alloy 2 (55 % and 51 % respectively) and alloy 3 (57 % and 60 % respectively). Alloy 2 reveals a tensile strength of about 1255 MPa for λ2 condition and 1009 MPa after tempering. Alloy 3 has a strength about 1186 MPa for λ2 without tempering and 951 MPa for the tempered microstructure. The impact energy for the λ2 conditions is at about 48.4 J for alloy 3 and below 35 J for alloy 1 and 30 J for alloy 2. The total elongation of alloy 3 with cooling condition λ2 is by far highest at about 14.8 %. The values for the yield-to-tensile ratio from as quenched and continuously cooled condition are close to 0.7 and 0.75. Values for seamless steel pipe-applications with bainitic and martensitic microstructures are typically in the range between 0.7 and 0.8 [14].

For the carbide free bainitic microstructures, alloy 1 is most vulnerable to sour gas and hydrogen cracking with a CSR at 24 %. Alloy 2 has a CSR close to 10 % and alloy 3 close to 7 %. For sour gas resistance, the amount of the retained austenite is decisive. Austenite can be seen as a hindrance, it lowers the diffusion of hydrogen significantly. At lower temperatures, the austenite lattice sites behave like traps. There is too less thermal energy to overcome the energy barrier for hydrogen diffusion in austenite [15]. Investigations from Lee et.al. [16] and Choo et.al. [17] have shown, that the capability of austenite to hold hydrogen atoms is stronger than for dislocations. This is why they accumulate at the boundaries and recombines there [18]. As a consequence, morphologies with higher retained austenite content are less resistant against hydrogen induced cracking. Finally all tempered morphologies show a better HIC resistance than in the directly cooled conditions. This leads to the assumption, that the residual stresses may also influence the hydrogen behaviour of the material. It should be noted that the CSR value in this case is only to classify and rank the materials and morphologies. Seamless steel tubes for industrial applications need a HIC resistance of 0 % CSR for accreditation.

The observation for the transition temperature is listed in table 4. It should be noted, that the carbide free morphology (continuous cooling condition λ2) has a much higher transition temperature than with the as quenched and the tempered heat treatments. The other heat treatments fulfil the requirements as described in chapter 1 [5].

Table 3. Mechanical properties, tensile strength (TS), reduction of area (Z), total elongation (A_{50}), crack sensitive ratio (CSR), impact energy (KV) and yield-to-tensile ratio (YS/TS).

Heat treatment conditions	TS [MPa]	Z [%]	A_{50} [%]	CSR [%]	KV [J]	YS/TS [-]
Alloy 1						
as quenched	1675	39.8	11.0	2.4	28.4 ±1,4	0.74
λ2	1413	51.9	9.6	24.1	34.4 ±4,0	0.69
λ2&T 700°C 10’	1043	47.4	10.5	2.9	55.2 ±4,0	0.89
Q&T 700°C 10’	1047	57.7	11.1	4.8	56.3 ±1,2	0.90
Alloy 2						
as quenched	1785	42.5	9.6	1.4	28.2 ±1,2	0.76
λ2	1255	54.7	11.7	9.9	29.1 ±3,2	0.75
λ2&T 700°C 10’	1009	51.2	11.6	2.0	45.6 ±8,7	0.84
Q&T 700°C 10’	1012	54.2	11.0	1.4	64.5 ±1,2	0.90
Alloy 3						
as quenched	1480	38.7	6.1	0.6	39.7 ±1,4	0.75
λ2	1186	56.9	14.8	7.2	48.4 ±0,9	0.74
λ2&T 700°C 10’	951	59.6	12.6	3.2	41.1 ±8,9	0.87
Q&T 700°C 10’	971	55.8	12.9	5.1	82.6 ±3,0	0.90

Table 4. Transition temperature.

Heat treatment	Alloy 1	Alloy 2	Alloy 3
as quenched	-16 °C	-27 °C	-35 °C
λ2	-10 °C	14 °C	-24 °C
λ2 tempered 700°C 10’	-27 °C	-37 °C	-11 °C
Q&T 700°C 10’	-36 °C	-60 °C	-48 °C

5. Conclusion

Three low-alloy steels and their suitability for OCTG-applications were compared quantitatively. The alloy-concepts were strictly designed to ensure the desired microstructures. The laboratory heat treatment simulations follow commonly used industrial heat treatment routes in the field of seamless steel production. The as quenched heat treatments can be realized with an accelerated pipe cooling system. The alignment of a certain amount of pipes on the rake type cooling bed influences the continuous cooling time and further bainitic morphologies of a single pipe. A denser assignment leads to slower cooling rates of the pipes and further different morphologies. The comparison between the high strength morphologies have shown, that ultimate tensile strengths close to 1200 MPa with total elongations close to 15 % and reduction of area of about 55 % can be realized. Increasing the strength up to 1800 MPa with ductility values close to 40 % is easy to fulfil. Further, investigations to compare morphologies and classify them regarding the hydrogen resistance were done. It is shown, that the carbide free microstructures do not lead to a sufficient better result in case of hydrogen embrittlement as originally proposed. The mixed microstructures with martensitic/ bainitic-phases show however an excellent strength and toughness behaviour. It can be postulated that the retained austenite and the residual stresses have a major influence on the hydrogen induced cracking.

Acknowledgements

Financial support by the Austrian Federal Government (in particular from Bundesministerium für Verkehr, Innovation und Technologie and Bundesministerium für Wissenschaft, Forschung und Wirtschaft) represented by Österreichische Forschungsförderungsgesellschaft mbH and the Styrian and the Tyrolean Provincial Government, represented by Steirische Wirtschaftsförderungsgesellschaft mbH and Standortagentur Tirol, within the framework of the COMET Funding Programme is

gratefully acknowledged. Special thanks to Mrs. Dr. Spiradek-Hahn and Mr. Ing. Manfred Brabetz from the Montanuniversitaet Leoben for material characterizations with TEM. The authors gratefully acknowledge to the industrial-partners voestalpine tubulars GmbH & Co KG and RAG Rohöl-Aufsuchungs Aktiengesellschaft for support and discussion.

References

[1] Bleck W 2014 Advanced High Strength Steels for the automotive industry – from microstructures to nanostructures *stahl und eisen* 134 **7** 25-34, 2014
[2] Wirtschaftsvereinigung Stahlrohre e.V.: http://www.wv-stahlrohre.de/markt.html (22.01.2015)
[3] md/k 2014 Frackingboom und Schwellenländer treiben Stahlrohrnachfrage *stahl und eisen* 134 **3** 20-22
[4] Winter G, Klarner J, Keckes J and Buchmayr B 2015 *Proc. XXXIV. Verformungskundliches Kolloquium (Zauchensse)* (Chair of Metal Forming, Montanuniversitaet Leoben) p 203-209
[5] Kern A, Schriever U and Steinbeck G 2010 *Proc. of the Twentieth (2010) International Offshore and Polar Engineering Conference* (Beijing) ISBN 978-1-880653-77-7 (Set)
[6] Klarner J 2009 Thermomechanische Behandlung beim Walzen von nahtlosen Stahlrohren *PhD Thesis*
[7] Klarner J, Buchmayr B and Rainer W 2011 *BHM* 156 **5** 168–174
[8] Gomez G, Perez T, Bhadeshia H K D H 2009 *Mater. Sci. Technol.* **25** 1508-1512
[9] Zapffe C A 1941 Hydrogen embrittlement, internal stress and defects in steel *AIME 145* 225–271
[10] Song E J, Bhadeshia H K D H, Suh D 2013 Effect of hydrogen on the surface energy of ferrite and austenite *Corrosion Science* **77** 379–384
[11] Buchmayr B 2002 *Werkstoff – und Produktionstechnik mit Mathcad, Modellierung und Simulation* Springer (Berlin) 3-540-43014-8
[12] NACE Standard TM0284-2011 Item No. 21215 *Evaluation of Pipeline and Pressure Vessel Steels for Resistance to Hydrogen-Induced Cracking,* 2011.
[13] Sackl S, Clemens H and Primig S 2015 Investigation of the Self Tempering Effect of Martensite by Means of Atom Probe Tomography *PM 52* **7** 374-383
[14] Gomez R, Pérez T E, Bhadeshia H 2010 High strength bainitic steel for OCTG applications, Patent US 2010/0294401 A1
[15] Park Y D, Maroef I S, Landau A, Olson D L 2002 Retained austenite as a hydrogen trap in steel welds *Welding Journal* 27–35
[16] Lee H G and Lee J Y 1984 Hydrogen trapping by TiC particels in iron *Acta Metall.* **32** (1) 131-136
[17] Choo W Y and Lee J Y 1982 Thermal analysis of trapped hydrogen in pure iron *Metall. Trans* A **13** A 135-140
[18] Fielding L, Song E, Han D, Bhadeshia H K D H 2014 Hydrogen diffusion and the percolation of austenite in nanostructured bainitic steel *Proceedings of the Royal Society* A **470** 1–32